

## GRAVITY DARKENING AND BRIGHTENING IN BINARIES

HELEN E. WHITE<sup>1</sup>, THOMAS W. BAUMGARTE<sup>1,2</sup> AND STUART L. SHAPIRO<sup>2,3</sup>

<sup>1</sup> Department of Physics and Astronomy, Bowdoin College, Brunswick, ME 04011

<sup>2</sup> Department of Physics, University of Illinois at Urbana-Champaign, Urbana, IL 61801 and

<sup>3</sup> Department of Astronomy and NCSA, University of Illinois at Urbana-Champaign, Urbana, IL 61801

*Draft version October 18, 2018*

### ABSTRACT

We apply a von Zeipel gravity darkening model to corotating binaries to obtain a simple, analytical expression for the emergent radiative flux from a tidally distorted primary orbiting a point-mass secondary. We adopt a simple Roche model to determine the envelope structure of the primary, assumed massive and centrally condensed, and use the results to calculate the flux. As for single rotating stars, gravity *darkening* reduces the flux along the stellar equator of the primary, but, unlike for rotating stars, we find that gravity *brightening* enhances the flux in a region around the stellar poles. We identify a critical limiting separation beyond which hydrostatic equilibrium no longer is possible, whereby the flux vanishes at the point on the stellar equator of the primary facing the companion. For equal-mass binaries, the total luminosity is reduced by about 13% when this limiting separation is reached.

*Subject headings:* binaries: close – stars: rotation

### 1. INTRODUCTION

Early studies (von Zeipel 1924a,b,c; Chandrasekhar 1933) showed that on stellar surfaces the radiative flux is proportional to the effective gravitational force (see, e.g., Kippenhahn & Weigert 1990; Tassoul 2000, for reviews). In rotating stars, this means that regions close to the pole are brighter (and have a higher effective temperature) than regions close to the equator, an effect that is often referred to as *gravity darkening*. In fact, for stars rotating at the break-up speed, the radiative flux vanishes at the equator (see, e.g., Baumgarte & Shapiro 1999, hereafter Paper I). Gravity darkening plays an important role in the classification of stars (e.g. Maeder & Peytremann 1970), and may even provide a means of estimating stellar masses independently of binary companions (Zhao et al. 2009).

While the simplest gravity darkening models make several assumptions that restrict their applicability to very massive and supermassive stars (as we will review in Section 2 below), they continue to be useful in a number of different contexts. Cranmer & Owocki (1995), for example, adopt similar models to compute radiative fluxes and driving forces for winds from rapidly rotating B stars. In Paper I, two of us adopted a simple Roche model to determine the envelope structure of and emergent radiation flux from a rotating, supermassive star (SMS) and employed the results to calculate the evolutionary timescale for these objects.

An exciting recent development provides a new motivation for studying gravity darkening. With optical or infrared interferometric arrays (including the PTI, NPOI and CHARA arrays), it has become possible to obtain resolved interferometric images of individual stars (e.g. van Belle et al. 2001; Peterson et al. 2006; Aufdenberg et al. 2006). Observations of rotating stars, which indeed show oblate shapes with brighter poles and darker equators, are analyzed using gravity darkening models. These models can be used to relate different stellar features to each other, for example the ratio between the polar and

equatorial fluxes to the star’s angular velocity. While some deviations between observations and models point to the fact that some of the assumptions made in the models may be too restrictive (for example, the observed stars may have complicated surface layers or differential rotation; see, e.g., Monnier et al. (2007) as well as Section 7 of Zhao et al. (2009) for discussions), the basic features are represented reasonably well. Moreover, the quality of fits can be improved by introducing additional free parameters into the models (for other model improvements see, e.g., Espinosa Lara & Rieutord (2011) and Claret (2012)).

In addition to observations of rotating stars, resolved interferometric images of close binary stars have become available (Zhao et al. 2008). While these observations do not yet have sufficient resolution to distinguish detailed models, they do motivate a study of gravity darkening in binaries.

In this short paper we point out that, under the assumptions listed in Section 2, the simple gravity darkening models for rotating stars can be generalized very easily to describe corotating stars in a binary system. As a consequence, we obtain very simple analytical expressions for the envelope structure, flux and the total luminosity for a massive or supermassive primary orbiting a point-mass secondary as a function of the binary separation and mass ratio. While the effects of rotation always decrease the surface flux (compared to a nonrotating star in isolation), the presence of a binary companion decreases the flux in some regions of the star, but increases the flux in a region around the pole. In a binary, we therefore encounter both gravity darkening and gravity brightening. We also identify a critical limiting separation below which hydrostatic equilibrium cannot exist and at which the surface flux from the point on the stellar equator facing the binary companion vanishes. For an equal-mass binary, the total luminosity is reduced by about 13% once this separation has been reached.

Elements of this problem have been known for a long

time (e.g. von Zeipel 1924c; Osaki 1965) and the model we construct presumably will be superseded by more detailed numerical treatments. We nevertheless hope that our simple analysis and analytical expressions may prove useful, for instance, in providing preliminary interpretations of future resolved images of close binary stars and calibrating more detailed numerical models.

Our paper is organized as follows. In Section 2 we review our basic assumptions. In Section 3 we review the Roche approximation and its application to binaries to determine the envelope structure and locate the surface of corotating stars in a binary. In Section 4 we compute the radiative flux from these stars, and find both gravity darkening and brightening. We integrate this flux to find the total luminosity in Section 5 and conclude with a brief discussion in Section 6.

## 2. BASIC ASSUMPTIONS

Our analysis of a binary relies on several explicit assumptions. Some of these assumptions we already adopted in Paper I, where we treated uniformly rotating, highly massive stars and SMSs in isolation. To determine the equilibrium structure of the envelope, we assume that the primary is

1. governed by Newtonian gravitation,
2. in synchronous orbit about a point-mass secondary, and that its envelope
3. is described by the Roche model,
4. is characterized by a polytropic equation of state, and
5. interacts with the secondary via a potential that can be truncated beyond the quadrupolar tidal term.

To determine the emergent radiative flux from the primary, we further assume that its envelope is

6. dominated by thermal radiation pressure,
7. fully convective, and
8. characterized by a constant Rosseland mean opacity (e.g., electron scattering).

We assume that gravitational fields are sufficiently weak so that we can apply Newtonian gravity. This assumption clearly holds for normal stars. SMSs of greatest astrophysical interest have masses and radii that satisfy  $R/M \gtrsim 400$  so that this assumption certainly holds. Relativistic corrections are important for the stability of SMSs, but can be neglected in the analysis of the equilibrium state.

The assumption that the binary is in corotation follows from the observation that most short period binaries containing massive stars orbit in circular, synchronous orbits (Vanbeveren et al. 1998). The combination of convection and magnetic fields are likely to generate an effective turbulent viscosity, which dampens nonsynchronous motion and brings the binary into corotation.

The assumption of a point-mass companion is adopted for simplicity. If the corotating companion is also a massive star, the point-mass can be replaced by a finite star whose envelope can be treated identically to the envelope of the primary. The results for the companion's envelope structure and emergent flux would depend the same way on its mass and radius as we find for the primary. We truncate the potential of the secondary after the quadrupolar tidal term, which captures the leading-order, dominant effects of the secondary on the primary.

For large masses, the ratio between radiation pressure,  $P_r$ , and gas pressure,  $P_g$ , satisfies

$$\beta_P \equiv \frac{P_g}{P_r} = 8.49 \left( \frac{M}{M_\odot} \right)^{-1/2} \quad (1)$$

(see, e.g., eqs. (17.2.8) and (17.3.5) in Shapiro & Teukolsky 1983); here the coefficient has been evaluated for a composition of pure ionized hydrogen. For SMSs with  $M \gtrsim 10^4 M_\odot$ , we can therefore neglect the pressure contributions of the plasma in determining the equilibrium profile, even though the plasma may be important for determining the stability of the star (Zel'dovich & Novikov 1971; Shapiro & Teukolsky 1983). A simple proof that very massive stars or SMSs are convective in this limit has been given by Loeb & Rasio (1994).<sup>1</sup> This result implies that the photon entropy per baryon,

$$s_r = \frac{4}{3} \frac{aT^3}{n_B} \quad (2)$$

is constant throughout the star, and so therefore is  $\beta_P \approx 8(s_r/k)^{-1}$ . Here  $a$  is the radiation density constant,  $T$  is the temperature,  $n_B$  is the baryon density, and  $k$  is Boltzmann's constant. As a consequence, the equation of state of a very massive star or SMS is that of an  $n = 3$  polytrope:

$$P = K\rho^{4/3}, \quad K = \left[ \left( \frac{k}{\mu m} \right)^4 \frac{3(1 + \beta_P)^3}{a\beta_P^4} \right]^{1/3} = \text{const}, \quad (3)$$

where  $m$  is the atomic mass unit and  $\mu$  is the mean molecular weight (cf. Clayton 1983, eq. (2-289); note that Clayton adopts a different definition of  $\beta_P$ , which is related to ours by  $\beta_{\text{Clayton}} = \beta_P/(1 + \beta_P)$ ). In the high temperature, low density, strongly ionized plasma of a very massive or SMS, Thomson scattering off free electrons is the dominant source of opacity. This opacity is independent of density and justifies our assumption about the Rosseland mean opacity.

In applications to SMSs our analysis neglects electron-positron pairs and Klein-Nishina corrections to the electron-scattering opacity, which is valid for  $M \gtrsim 10^5 M_\odot$  (see, e.g. Fuller et al. 1986).

## 3. THE ROCHE MODEL FOR A BINARY

We begin with the equation of hydrostatic equilibrium satisfied by the primary,

$$\frac{\nabla P}{\rho} = -\nabla(\Phi_p + \Phi_c + \Phi_r). \quad (4)$$

<sup>1</sup> In fully convective stars energy transport in the stellar interior is dominated by convection. However, there is still an outgoing flux of radiation from the stellar surface. The latter is what we compute in Section 4 below.

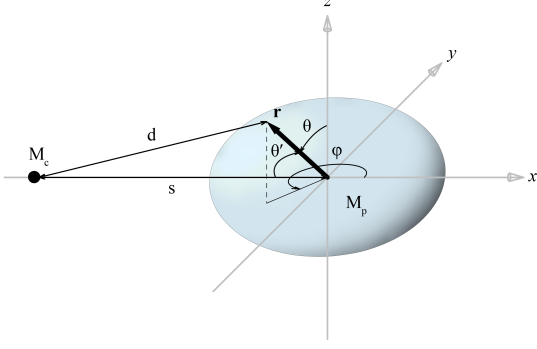


FIG. 1.— Sketch of the coordinate system used in our calculation. The primary of mass  $M_p$  is represented by the shaded configuration on the right, while the companion of mass  $M_c$  is represented by the dot on the left.

Here the right-hand side describes an effective gravitational force, which is derived from the (interior) gravitational potential  $\Phi_p$  of the primary, the (exterior) gravitational potential of the companion  $\Phi_c$ , and a centrifugal potential  $\Phi_r$  arising from the (synchronous) rotation of the primary.

Stars with soft equations of state are centrally condensed, i.e. most of the mass is concentrated in a high-density core that is surrounded by an extended low-density envelope. For an  $n = 3$  polytrope, for example, the ratio between central and mean density is  $\rho_c/\bar{\rho} = 54.2$ . The gravitational force in the envelope is therefore dominated by the massive core, and it is thus legitimate to neglect the self-gravity of the envelope. In the envelope, we may therefore approximate the Newtonian potential of the primary star  $\Phi_p$  as

$$\Phi_p = -\frac{M_p}{r} \quad (5)$$

where  $M_p$  is the mass of the primary and  $r$  the distance from the primary's center (here we adopt gravitational units by setting  $G \equiv 1$ ).

In accord with the Roche model, the companion may be treated as a point mass  $M_c$ , located at a distance  $s$  from the center of the primary (see Fig. 1). The potential at a point  $\mathbf{r}$  in the primary is then given by

$$\Phi_c = -\frac{M_c}{d}, \quad (6)$$

where  $d$  is the distance from  $M_c$ . We now expand  $d$  about  $s \geq r$ ,

$$\frac{1}{d} = \frac{1}{s} \sum_{\ell=0}^{\infty} \left(\frac{r}{s}\right)^{\ell} P_{\ell}(\cos \theta'), \quad (7)$$

where  $P_{\ell}(\cos \theta')$  is the Legendre polynomial of order  $\ell$ , and where  $\theta'$  is the angle between  $\mathbf{r}$  and the line connecting the center of the primary to the point mass companion. The first term  $\ell = 0$  is a constant that can be ignored. We will see that the  $\ell = 1$  term will cancel out later when we consider the rotational contribution  $\Phi_r$ , but we retain it for now. The first relevant term is the quadrupolar tidal term  $\ell = 2$ . Truncating the expansion (7) after this term we approximate

$$\Phi_c = -\frac{M_c r}{s^2} \cos \theta' - \frac{M_c r^2}{2s^3} (3 \cos^2 \theta' - 1). \quad (8)$$

We now introduce a coordinate system as shown in Fig. 1, so that the orbital plane is in the  $x - y$  plane, with the center of the primary at the origin and the companion at  $x = -s$  and  $y = z = 0$ . In terms of spherical polar coordinates we now express  $\cos \theta' = -x/r = -\cos \phi \sin \theta$ , and hence

$$\Phi_c = \frac{M_c x}{s^2} - \frac{M_c r^2}{2 s^3} (3 \cos^2 \phi \sin^2 \theta - 1). \quad (9)$$

Finally, the rotational potential  $\Phi_r$  in (4) arises from the rotation of the primary about the system's center of mass. Assuming corotation, so that the star appears static in the rotating frame of the binary, we may write this term as

$$\Phi_r = -\frac{1}{2} \Omega^2 ((x - x_{\text{CM}})^2 + y^2), \quad (10)$$

where

$$x_{\text{CM}} = -\frac{M_c}{M_p + M_c} s \quad (11)$$

is the location of the center of mass. Using (11) as well as Kepler's law

$$\Omega^2 = \frac{M_p + M_c}{s^3} \quad (12)$$

we can write (10) as

$$\Phi_r = -\frac{1}{2} \Omega^2 x_{\text{CM}}^2 - \frac{M_c x}{s^2} - \frac{1}{2} \frac{M_p + M_c}{s^3} r^2 \sin^2 \theta. \quad (13)$$

The first term on the right-hand side is a constant term that can be ignored. The second term will exactly cancel the first term in (9) when the two potentials are added in (4); we may therefore discard the linear terms in both (9) and (13). Our potentials  $\Phi_c$  and  $\Phi_r$  then reduce to

$$\begin{aligned} \Phi_c + \Phi_r = & -\frac{M_c r^2}{2 s^3} (3 \cos^2 \phi \sin^2 \theta - 1) \\ & -\frac{1}{2} \frac{M_p + M_c}{s^3} r^2 \sin^2 \theta. \end{aligned} \quad (14)$$

Integrating eq. (4) yields the Euler integral

$$h + \Phi_p + \Phi_c + \Phi_r = H, \quad (15)$$

where  $H$  is a constant of integration and where

$$h = \int \frac{dP}{\rho} = (n+1) \frac{P}{\rho} \quad (16)$$

is the enthalpy per unit mass. Evaluating (15) for infinite binary separation  $s \rightarrow \infty$  (where  $\Phi_c = \Phi_r = 0$ ) at the stellar surface (where  $h = 0$ ) we find

$$H = -\frac{M_p}{R_0}, \quad (17)$$

where  $R_0$  is the stellar radius for the nonrotating (spherical) star in isolation.

It is consistent with the Roche approximation to assume that the core remains unaffected by the presence of the binary companion. Given that  $\Phi_c$  and  $\Phi_r$  vanish at the center of the star, and given that we may assume  $h$  and  $\Phi_p$  to remain unperturbed there, we may also assume that  $H$  is independent of the binary separation, so that we can always express it in terms of  $R_0$  as in eq. (17). Similar arguments have been made for isolated

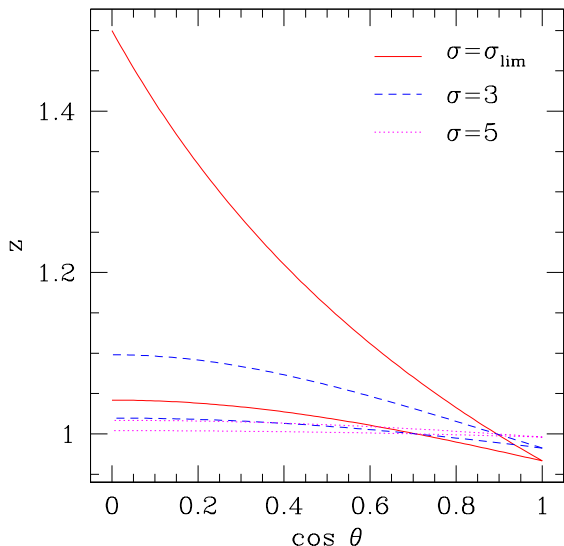


FIG. 2.— The dimensionless stellar radius  $z$  as a function of  $\cos \theta$  for an equal-mass binary ( $q = 1$ ) at different values of the binary separation  $\sigma$ . For each binary separation the top line represents results for  $\phi = \pi$  (i.e. in the direction toward the binary companion) while the bottom line represents results for  $\phi = \pi/2$ . The two lines connect at the pole ( $\cos \theta = 1$ ). Note that for  $\sigma = \sigma_{\text{lim}}$ , we have  $z = 3/2$  for the point facing the binary companion (see eq. (26)).

rotating stars (e.g. Zel’dovich & Novikov 1971; Shapiro & Teukolsky 1983), where they have been confirmed by numerical simulations (e.g. Papaloizou & Whelan 1973).

The surface of the star satisfies  $h = 0$  and can be determined from eq. (15) in the form

$$\Phi_p + \Phi_c + \Phi_r - H = 0. \quad (18)$$

Introducing dimensional parameters for the mass ratio

$$q \equiv \frac{M_c}{M_p}, \quad (19)$$

the binary separation

$$\sigma \equiv \frac{s}{R_0}, \quad (20)$$

and the distance from the stellar center to the surface

$$z \equiv \frac{r}{R_0}, \quad (21)$$

we can bring (18) into the form of a cubic equation for  $z$ ,

$$C_3 z^3 - z + 1 = 0, \quad (22)$$

where we have abbreviated

$$C_3 = \frac{1}{2\sigma^3} \left( q(3 \cos^2 \phi \sin^2 \theta - 1) + (1 + q) \sin^2 \theta \right). \quad (23)$$

Given binary parameters  $q$  and  $\sigma$ , this cubic equation can be solved analytically to find  $z$  as a function of the coordinates  $\theta$  and  $\phi$  (see Appendix).

Note that the cubic (22) takes exactly the same form as that for a single rotating star (see, eq. (23) in Paper I), except that the coefficient  $C_3$  is now different.<sup>2</sup> Instead of depending on  $\theta$  only, as for axisymmetric, rotating

<sup>2</sup> Our coefficient  $C_3$  reduces to the corresponding coefficient for rotating stars when  $q = 0$ .

stars, it now depends on both  $\theta$  and  $\phi$ . Moreover, for rotating stars the corresponding coefficient is nonnegative, resulting in values for  $z$  that are always greater than or equal to unity. Here, however,  $C_3$  can be positive or negative. At the poles, where  $\sin \theta = 0$ , for example, we have  $C_3 < 0$  (for finite  $\sigma$ ), resulting in  $z < 1$ . This is consistent with the fact that the tidal field of the companion leads to the squeezing of the primary along its poles and an elongation along its equator.

Hydrostatic equilibrium is only possible if, at the surface of the star, where the density vanishes, the pressure increases towards the interior of the star. Our sequences of hydrostatic equilibria therefore terminate when, at the point facing the companion, i.e. at  $\theta = \pi/2$  and  $\phi = \pi$ , the right-hand side of (4) vanishes.<sup>3</sup> Evaluating the right-hand side of (4) at that point, and setting it to zero, yields

$$(1 + 3q) \frac{z^3}{\sigma^3} = 1. \quad (24)$$

For  $\theta = \pi/2$  and  $\phi = \pi$  we also have

$$C_3 = \frac{1 + 3q}{2\sigma^3}. \quad (25)$$

Inserting (24) together with (25) into the cubic (22) we find that the limiting value of  $z$ , at  $\theta = \pi/2$  and  $\phi = \pi$ , is

$$z_{\text{lim}} = \frac{3}{2}. \quad (26)$$

Interestingly, this is the same value obtained for the equator of single stars rotating at the break-up limit (see, e.g., eq. (10) in Paper I). Inserting (26) back into (24) we now obtain the limiting binary separation  $\sigma_{\text{lim}}$  for which, under our assumptions, sequences of hydrostatic equilibria end,

$$\sigma_{\text{lim}} = \frac{3}{2} (1 + 3q)^{1/3}. \quad (27)$$

For a mass ratio of  $q = 1$ , for example, we have  $\sigma_{\text{lim}} \approx 2.38$ . Given that  $\sigma \gtrsim 2.4$  for all equilibrium models, our truncation of the interaction potential beyond the tidal term is justified in a first approximation. The corresponding Roche limit for a homogeneous, incompressible ( $n = 0$ ) star, allowing for departure of the angular velocity from the Keplerian value due to the ellipsoidal shape of the primary, yields  $\sigma_{\text{lim}} = 2.713$  (Lai et al. 1993).

In Fig. 2 we show results for  $z$  for an equal-mass binary for different values of the binary separation. In particular, these results confirm the limiting value (26) for the end point of the sequence at  $\sigma_{\text{lim}}$ .

#### 4. GRAVITY DARKENING AND BRIGHTENING

In the diffusion approximation, the radiation flux is given by

$$\mathbf{F} = -\frac{1}{3\kappa\rho} \nabla U, \quad (28)$$

where  $U$  is the energy density of the radiation,

$$U = aT^4 = 3P, \quad (29)$$

<sup>3</sup> Having truncated the expansion (7) after the tidal term, this point is equivalent to the point pointing away from the binary companion,  $\theta = \pi/2$  and  $\phi = 0$ .

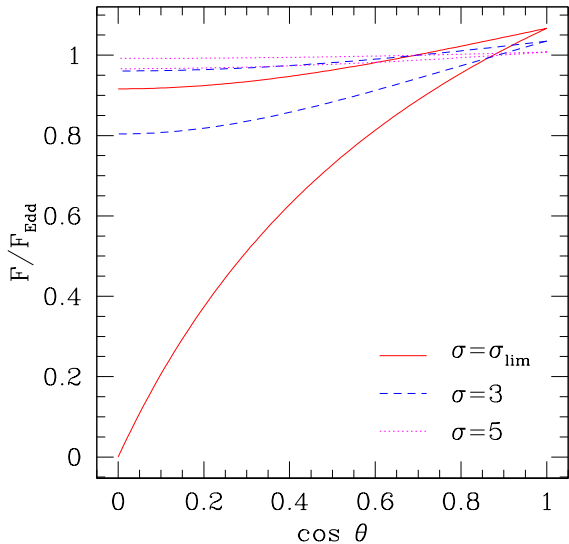


FIG. 3.— The flux  $F/F_{\text{Edd}}$  as a function of function of  $\cos \theta$  for an equal-mass binary ( $q = 1$ ) at different values of the binary separation  $\sigma$ . For each binary separation the bottom line represents results for  $\phi = \pi$  (i.e. in the direction toward the binary companion) while the top line represents results for  $\phi = \pi/2$ . The two lines connect at the pole ( $\cos \theta = 1$ ). Note that in a region around the pole the flux exceeds the corresponding Eddington flux, and that the flux vanishes at the point facing the binary companion when  $\sigma = \sigma_{\text{lim}}$ .

and where  $\kappa$  is the opacity (which we assume to be dominated by electron scattering,  $\kappa = \kappa_{\text{es}}$ ). We have also assumed that the pressure is dominated by radiation pressure

$$P \approx P_r = \frac{1}{3} a T^4. \quad (30)$$

Inserting equations (28) and (29) into the equation of hydrostatic equilibrium (4) yields

$$\kappa \mathbf{F} = \nabla(\Phi_p + \Phi_c + \Phi_r). \quad (31)$$

In polar coordinates in an orthonormal basis, the magnitude of the flux is

$$F = (F_{\hat{r}}^2 + F_{\hat{\theta}}^2 + F_{\hat{\phi}}^2)^{1/2}. \quad (32)$$

Evaluating the gradients of the potentials  $\Phi_p$ ,  $\Phi_c$  and  $\Phi_r$  we find

$$\begin{aligned} \frac{F}{F_{\text{Edd}}} = & \left\{ \left( 1 - \frac{q}{\sigma^3} z^3 (3 \cos^2 \phi \sin^2 \theta - 1) - \frac{1+q}{\sigma^3} z^3 \sin^2 \theta \right)^2 \right. \\ & + \left( \frac{q}{\sigma^3} z^3 (3 \cos^2 \phi \cos \theta \sin \theta) + \frac{1+q}{\sigma^3} z^3 \sin \theta \cos \theta \right)^2 \\ & \left. + \left( \frac{q}{\sigma^3} z^3 (3 \cos \phi \sin \phi \sin \theta) \right)^2 \right\}^{1/2} \end{aligned} \quad (33)$$

where

$$F_{\text{Edd}} = \frac{M_p}{\kappa r^2} \quad (34)$$

is the Eddington flux from a spherical star of radius  $r$ .

We graph the flux  $F$  for an equal-mass binary for different values of the binary separation  $\sigma = s/R_0$  in Fig. 3. In a region around the poles the flux is greater than the Eddington flux. The reason for this “gravity brightening” effect is that, at the poles, the tidal forces caused by

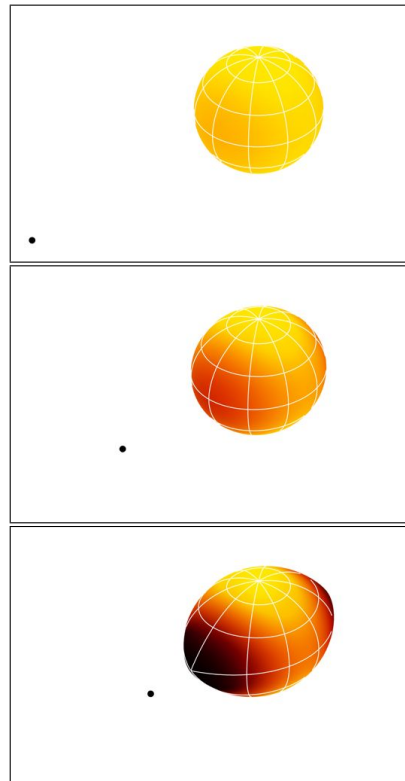


FIG. 4.— Surface images of the primary in an equal-mass binary at three different binary separations  $\sigma = 5$  (top panel),  $\sigma = 3$  (middle panel) and  $\sigma = \sigma_{\text{lim}}$  (bottom panel). The shape of the primary is given by eq. (22), while the color coding represents the flux (33). Yellow indicates the largest flux, red a smaller flux, and black a vanishing flux. The dot represents the point mass that models the companion.

the companion lead to an increase of the effective gravitational force, which in turn leads to an increase in the flux. The opposite is true at the points on the stellar equator either pointing directly toward the companion or directly away from the companion. At these points, the tidal forces lead to a reduction in the effective gravitational force. On the equator, stellar rotation also leads to a reduction of the effective gravitational force. At the two points facing towards or away from the companion (i.e. for  $\phi = \pi$  or  $\phi = 0$ ), the two effects act together to result in the greatest reduction in the brightness, i.e. the strongest gravity darkening effect. For the limiting binary separation  $\sigma = \sigma_{\text{lim}}$ , the flux completely vanishes at those points. At the two points on the equator with  $\phi = \pi/2$  and  $\phi = 3\pi/2$ , on the other hand, the two effects counteract, leading to a smaller reduction in the flux.

In Fig. 4 we also show surface images of the primary in an equal-mass binary at three different binary separations. The shape of the primary is given by eq. (22) and reflects the tidal deformation, while the color coding indicates the local radiative surface flux (33). Yellow indicates the largest flux, red a smaller flux, and black a vanishing flux.

## 5. LUMINOSITY

We find the total luminosity of the star by integrating the flux (33) over the stellar surface

$$L = \oint \mathbf{F} \cdot d\mathbf{A} = \oint F dA. \quad (35)$$

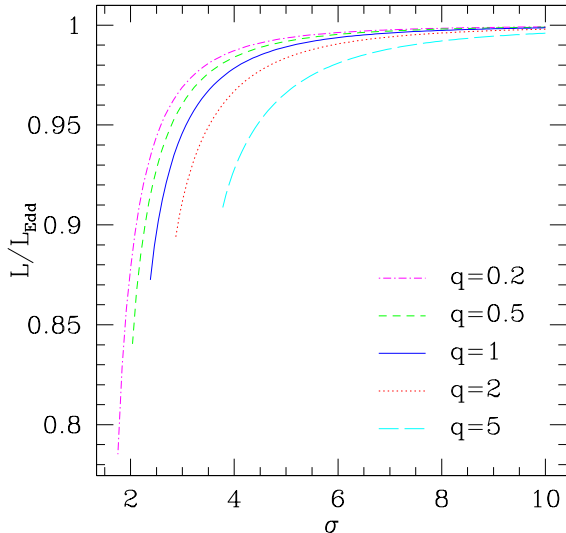


FIG. 5.— The luminosity  $L/L_{\text{Edd}}$  as a function of binary separation  $\sigma$  for different values of the mass ratio  $q$ . For each value of  $q$ , the sequences start at  $\sigma = 10$  and end at  $\sigma_{\text{lim}}$  given by eq. (27).

The surface element can be written as

$$d\mathcal{A} = \left\{ 1 + \frac{1}{z^2} \left( \frac{dz}{d\theta} \right)^2 + \frac{1}{z^2 \sin^2 \theta} \left( \frac{dz}{d\phi} \right)^2 \right\}^{1/2} r^2 d\Omega, \quad (36)$$

where  $d\Omega = \sin\theta d\theta d\phi$ . We then insert the flux (33) and evaluate the integration numerically to find the star's luminosity  $L$ . It is convenient to divide the result by the Eddington luminosity

$$L_{\text{Edd}} = \frac{4\pi M}{\kappa} \quad (37)$$

and express the results in terms of the dimensionless ratio  $L/L_{\text{Edd}}$ . In Fig. 5 we show results for the luminosity as a function of the binary separation  $\sigma$  for different values of the mass ratio  $q$ . All sequences shown start at  $\sigma = 10$  and end at the limiting binary separation  $\sigma_{\text{lim}}$  given by eq. (27). For an equal-mass binary, for example, the luminosity is reduced by about 12.7% when the binary reaches  $\sigma_{\text{lim}}$ . We also verified that in the limit  $q \rightarrow 0$ , the luminosity for  $\sigma = \sigma_{\text{lim}}$  is reduced by about 36%, which is the value found for single stars rotating at the break-up limit (see, e.g., Paper I).

## 6. DISCUSSION

We apply gravity darkening models to corotating binary stars and obtain simple and analytical expressions for the surface flux of tidally distorted stars. The tidal

interaction leads to both gravity darkening (along the equator) and gravity brightening (in regions around the poles). We identify a critical separation at which, within the Roche model, sequences of hydrostatic equilibrium end, and at which the radiative flux at the point on the equator that faces the binary companion vanishes. At this critical separation, the total luminosity in an equal-mass binary is about 13% less than for the corresponding nonrotating star in isolation.

Simple and analytical models for the flux and luminosity from binary stars, even if they are approximate, are useful in many ways. In particular, we hope that they will provide useful models for comparison with future resolved interferometric images of close binary stars. For single rotating stars, von Zeipel gravity darkening models capture the basic features of interferometric images reasonably well, but they also show some deviations. Presumably, these deviations are caused by the fact that some of the assumptions do not apply to the observed stars. In particular, many main sequence stars have complicated surface layers or rotate differentially rather than uniformly. As discussed by Monnier et al. (2007) (see also Zhao et al. 2009), the agreement between model and observations can be improved by introducing new free parameters. Monnier et al. (2007) and others have used “ $\beta$ -free” models, in which the effective temperature is taken to be  $T_{\text{eff}} \propto g_{\text{eff}}^\beta$ , where  $g_{\text{eff}}$  is the effective gravitational force on the right-hand side of eq. (4). In the “standard” model,  $\beta = 1/4$ , but allowing  $\beta$  to be a free parameter allows for improved fits to the observations. Other improvements to the simple von Zeipel models have been proposed by Espinosa Lara & Rieutord (2011) and Claret (2012). We expect that similar generalizations may improve future fits between binary gravity darkening models and observations as well.

It is a pleasure to thank Andrew Currier for producing Figs. 1 and 4 for us. HEW gratefully acknowledges support through a Clare Boothe Luce undergraduate fellowship. This work was supported in part by NSF Grant PHY-1063240 to Bowdoin College and by NSF Grant PHY-0963136 as well as NASA Grant NNX10AI73G at the University of Illinois at Urbana-Champaign.

## APPENDIX

### SOLUTION FOR THE STELLAR SURFACE

In this brief appendix we present the solution to the cubic equation (22), yielding the stellar surface  $z$ . The general solution to a cubic equation can be found, for example, in Press et al. (2007). Applying their prescription to our equation (22), we see that the form of the solution  $z$  depends on the coefficient  $C_3$ .

By combining equations (23) and (27) we first observe that we always have  $C_3 \leq 4/27$ . The form of the solution then depends only on the sign of  $C_3$ . If  $C_3$  is positive, then the cubic has three real roots and we pick the one that yields  $z = 1$  when  $C_3 = 0$ , given by

$$z = -\frac{2}{\sqrt{3C_3}} \cos \left( \frac{\arccos(\sqrt{27C_3/4}) - 2\pi}{3} \right) \quad (C_3 \geq 0). \quad (\text{A1})$$

For a single, rotating star, we always have  $0 \leq C_3 \leq 4/27$  (see, e.g., Paper I), so that the solution can always be written in this form. For a binary, however,  $C_3$  can also be negative. In this case, the cubic has one real and two imaginary roots. Defining

$$A = \left( \frac{1}{2|C_3|} \left\{ \left( 1 + \frac{4}{27|C_3|} \right)^{1/2} + 1 \right\} \right)^{1/3} \quad (\text{A2})$$

we can write the real root as

$$z = A - \frac{1}{3|C_3|A} \quad (C_3 < 0). \quad (\text{A3})$$

## REFERENCES

- Aufdenberg, J. P., et al., 2006, *ApJ*, 645, 664  
 Baumgarte, T. W. & Shapiro, S. L., 1999, *ApJ*, 526, 937 (Paper I)  
 van Belle, G. T., et al., 2001, *ApJ*, 559, 1155  
 Chandrasekhar, S., 1933, *MNRAS*, 93, 462  
 Claret, A., 2012, *A&A*, 538, 3  
 Clayton, D., 1983, *Principles of Stellar Evolution and Nucleosynthesis* (University of Chicago Press)  
 Cranmer, S. R. & Owocki, S. P., 1995, *ApJ*, 440, 308  
 Espinosa Lara, F. & Rieutord, M., 2011, *A&A*, 533, 43  
 Fuller, G. M., Woosley, S. E., & Weaver, T. A., 1986, *ApJ*, 307, 675  
 Kippenhahn, R. & Weigert, A., 1990, *Stellar Structure and Evolution* (Springer Verlag)  
 Lai, D., et al., 1993, *ApJS*, 88, 228  
 Loeb, A., and Rasio, F. A., 1994, *ApJ*, 432, 52  
 Maeder, A. & Peytremann E., 1970, *A&A*, 7, 120  
 Monier, J. D., et al., 2007, *Science*, 317, 342  
 Osaki, Y., 1965, *PASJ*, 17, 97  
 Papaloizou, J. C. B., & Whelan, F. A. J., 1973, *MNRAS*, 164, 1  
 Peterson, D. M., et al., 2006, *Nature*, 440, 896  
 Press, W. H., et al., 2007, *Numerical Recipes: The Art of Scientific Computing*, 3rd Edition (Cambridge University Press)  
 Shapiro, S. L. & Teukolsky, S. A., 1983, *Black Holes, White Dwarfs and Neutron Stars: The Physics of Compact Objects* (New York: Wiley)  
 Tassoul, J.-L., 2000, *Stellar Rotation* (Cambridge University Press)  
 Vanbeveren, D., et al., 1998, *The brightest binaries* (Kluwer Acad. Pub., Dordrecht)  
 Zhao, M., et al., 2008, *ApJ*, 684, L95  
 Zhao, M., et al., 2009, *ApJ*, 701, 209  
 von Zeipel, H., 1924, *MNRAS*, 84, 665  
 von Zeipel, H., 1924, *MNRAS*, 84, 684  
 von Zeipel, H., 1924, *MNRAS*, 84, 702  
 Zel'dovich, Ya. B. & Novikov, I. D., 1971, *Relativistic Astrophysics*, Vol. 1 (Univ. Chicago Press)